Sensitive ultrashort pulse chirp measurement

Daniel A. Bender, Michael P. Hasselbeck, and Mansoor Sheik-Bahae

*Department of Physics and Astronomy, Optical Science and Engineering Program, University of New Mexico,
Albuquerque, New Mexico 87131*

The chirp of an ultrashort laser pulse can be extracted with high accuracy from a modified spectrum auto-interferometric correlation waveform by using a new time domain algorithm that allows signal averaging. We display results revealing high sensitivity to chirp even with signal-to-noise levels approaching unity. Correction algorithms have been developed to accommodate signal distortion arising from bandwidth limitations, interferometer misalignment, and nonquadratic detector response. © 2006 Optical Society of America
OCIS codes: 320.7100, 140.7090.

The need to characterize ultrashort laser pulses has become increasingly important as the field of ultrafast science evolves. Existing schemes have been successful in completely resolving the instantaneous phase and field of the pulse.[1,2] Other methods center on temporal asymmetry in the pulse.[3] For many applications, however, a simpler, real-time measurement technique for pulse-width and frequency chirp assessment is desirable. Chirp can be examined by using a traditional second-order interferometric autocorrelation (IAC) trace,[4] but the sensitivity is poor. It has recently been shown that chirp can be determined accurately from the IAC trace by means of spectral reshaping.[5] This technique, which is called modified spectrum autointerferometric correlation (MOSAIC), is much simpler than phase-retrieval approaches because no additional hardware is needed beyond that used to obtain the IAC. MOSAIC uses spectral filtering of the IAC to render a waveform that is highly sensitive to chirp. Signal processing is simple and straightforward, allowing chirp characterization to be performed by a PC in real time.

We report a new implementation of MOSAIC that allows for significantly enhanced performance in the following ways: (i) accurate chirp measurement is possible with signals close to the noise level and with IAC fringe jitter, (ii) bandwidth-limited detection and nonquadratic response are automatically corrected, (iii) the order of the chirp can be determined (for a known functional form of the pulse profile), and (iv) algorithm efficiency is improved.

A MOSAIC is obtained by spectrally filtering the second-order IAC waveform. The Fourier transform spectrum of the second-order IAC reveals frequency components centered at 0, ω_0, and $2\omega_0$, where ω_0 is the fringe frequency. Spectral reshaping is performed by removing the ω_0 component, amplifying the $2\omega_0$ component by a factor of 2, and retaining the unmodified envelope component. An inverse Fourier transform is then performed, and the resulting waveform is a MOSAIC trace. A chirp-free MOSAIC trace exhibits a flat baseline, while the presence of shoulders indicates chirp.[5,6] Spectral reshaping can equivalently be accomplished in a more computationally efficient manner in the time domain by using the MOSAIC envelope method detailed here. Algorithm

efficiency has been improved by more than a factor of 2 when compared with the double-FFT scheme. In the present implementation, two curves define the MOSAIC; these curves are the maximum and minimum envelopes, both of which are depicted in Figs. 1(b) and 1(d). It is important to note that all the crucial chirp information is contained in the minimum envelope of each MOSAIC waveform. We also replace the maximum envelope of MOSAIC as defined in Ref. 5 by the intensity autocorrelation. In this new representation, the lower trace contains chirp information, while the upper trace conveys pulse duration only. Displaying individual interference fringes as described in Ref. 5 is not necessary to realize the high sensitivity of this technique.

The fringe-resolved MOSAIC trace is given by[5]

$$S_{\mathrm{MOSAIC}}(\tau) = g(\tau) + [g_s^2(\tau) + g_c^2(\tau)]^{1/2} \cos[2\omega\tau + \Phi(\tau)],\tag{1}$$

where $g(\tau) = \int f(t)f(t+\tau)\mathrm{d}t$ is the usual intensity autocorrelation that defines the pulse width,

$$\Phi(\tau) = -\tan^{-1}(g_s/g_c),\tag{2}$$

$$g_s(\tau) = \int f(t)f(t+\tau)\sin[2\Delta\phi(t)]\mathrm{d}t,\tag{3}$$

$$g_c(\tau) = \int f(t)f(t+\tau)\cos[2\Delta\phi(t)]\mathrm{d}t.\tag{4}$$

The intensity of the pulse is denoted $f(t)$, and $\Delta\phi(t) = \phi(t+\tau) - \phi(t)$ is the temporal chirp. The lower boundary of the MOSAIC envelope $S_{\min}$ defines shoulders that indicate the amount of chirp. This envelope is given by

$$S_{\min}(\tau) = g(\tau) - [g_s(\tau)^2 + g_c(\tau)^2]^{1/2}.\tag{5}$$

It is desirable to experimentally obtain $S_{\min}$ directly by eliminating the fringes. This can be done through the new spectral manipulation algorithm presented here. The needed quantities in Eq. (5) are extracted from the IAC signal by the homodyne operations $g_s(\tau) = 2\langle S_{\mathrm{IAC}}(\tau)\sin(2\omega_0\tau)\rangle_\Omega$ and $g_c(\tau) = 2\langle S_{\mathrm{IAC}}(\tau)\cos(2\omega_0\tau)\rangle_\Omega$; additionally, $g(\tau) = \langle S_{\mathrm{IAC}}(\tau)\rangle_\Omega/2$ is the intensity autocorrelation and
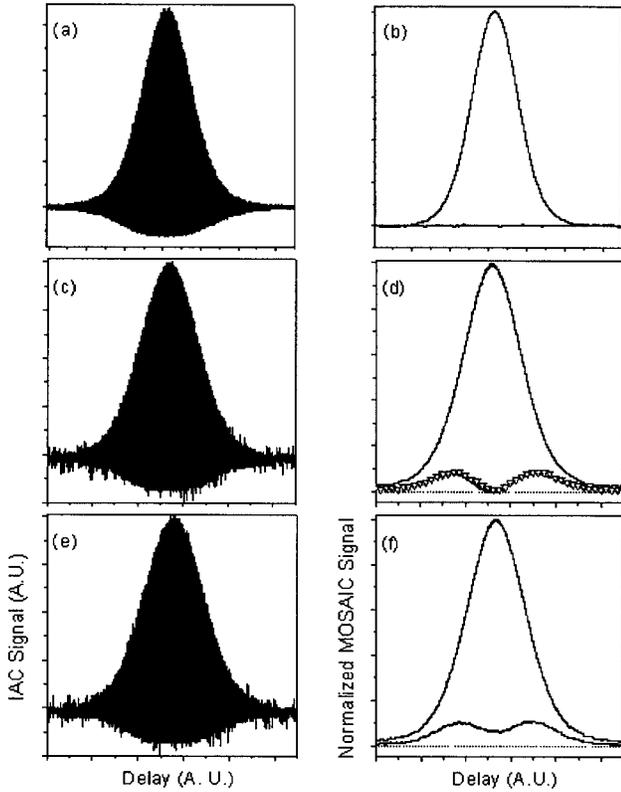
Fig. 1. Experimentally obtained IAC traces of an (a) unchirped pulse, (c) a chirped pulse, and (e) a chirped pulse with distortion. The distortion is produced by misaligning the autocorrelator. Corresponding MOSAIC maximum and minimum envelopes are shown in (b), (d), and (f). The corrected minimum envelope of the MOSAIC is depicted in (d) with triangles.

$S_{\mathrm{IAC}}(\tau)$ is the second-order interferometric autocorrelation signal. The brackets indicate low-pass filtering, and the upper cutoff frequency, Ω, is chosen based on the bandwidth of the pulse. In practice, $\omega_0/mN \leq \Omega\omega_0/2$, where N is the number of fringes in the FWHM of the second-order IAC and $1 \leq m \leq 6$. High-frequency fringes are therefore removed to display only the waveform envelope, which can be directly averaged.

We obtain the fringe frequency ω_0 in a time window at the peak of the IAC. When the signal-to-noise ratio approaches unity, an accurate measurement of ω_0 is no longer possible. The fundamental frequency ω_0 can, however, be determined with high accuracy even if the second-order autocorrelation signal is weak and noisy. A small fraction of the interferometer output is directed to a linear detector to generate a first-order IAC from which ω_0 can be obtained. This independent measurement of ω_0 allows very noisy IAC signals to be averaged in the MOSAIC algorithm and automatically corrected for distortion. This is accomplished by averaging Eq. (5) as follows:

$$\{S_{\mathrm{min}}(\tau)\}_{\mathrm{ave}} = \overline{g(\tau)} - \eta [\overline{g_s(\tau)^2 + g_c(\tau)^2}]^{1/2}, \qquad (6)$$

where η is a distortion correction factor that is generated by the algorithm. The IAC may be distorted as a result of detector bandwidth limitations, autocorr-

elator misalignment, and/or nonquadratic detector response leading to $S_{\mathrm{min}} \neq 0$ at $\tau=0$. The distortion correction factor makes chirp interpretation straightforward in MOSAIC. The coefficient η forces $\overline{S_{\mathrm{min}}}$ to zero at zero delay:

$$\eta = \frac{\overline{S_{\mathrm{min}}(0)}}{[\overline{g_0(0)^2 + g_c(0)^2}]^{1/2}} . \qquad (7)$$

This correction coefficient allows MOSAIC to separate pulse chirp information from distortion associated with autocorrelator misalignment and noise in the detection electronics.

An example of autocorrelator misalignment distortion is demonstrated experimentally in Fig. 1. We use a mode-locked Ti:sapphire laser producing 120 fs pulses at a center wavelength of 820 nm. An aligned IAC signal is shown in Fig. 1(c), while Fig. 1(e) depicts a signal from a deliberately misaligned autocorrelator. The spatial fringes across the detector mimic a restrictive electronic bandwidth. Corresponding MOSAIC waveforms are displayed in Figs. 1(d) and 1(f). The IAC traces before and after the misalignment appear identical. The MOSAIC signal in Fig. 1(f), however, reveals misalignment by a visible departure of S_{min} from the baseline at zero delay. It is important to eliminate such deviations for correct chirp characterization. Real-time calculation of η is performed by using Eq. (7); the corrected MOSAIC shown in Fig. 1(d) reproduces the undistorted shoulder height to within the measurement noise. MOSAIC can produce a correct shoulder height for nonquadratic detectors with $I^{2+\varepsilon}$, $-0.2 \leq \varepsilon \leq 0.2$ for chirped pulses producing a shoulder height of 13% or less with an error of ±2%. Equivalently, MOSAIC can determine the order of detection to within 7% for $-0.3 \leq \varepsilon \leq 1.0$ by using unchirped pulses. Our simulations show that MOSAIC can simultaneously correct for small insufficiencies in bandwidth, autocorrelator misalignment, and nonquadratic response in real time and with high accuracy.

The MOSAIC generation process with a very noisy IAC is demonstrated in Fig. 2. The IAC waveform is barely visible above the noise in Fig. 2 (left). After an implementation of the algorithm in Eq. (6), where an average has been taken over 1200 envelopes, a clear MOSAIC waveform can be resolved in Fig. 2 (right, triangles). This MOSAIC trace reproduces the chirp extracted from a noise-free IAC of the same pulse
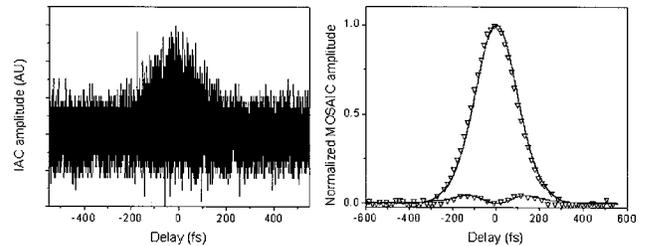

Fig. 2. Left, single IAC trace just above the noise level. Right, averaged MOSAIC waveform produced after acquiring 1200 noisy IAC traces (triangles); the chirp of the same pulse obtained with negligible noise is reproduced (solid curve).
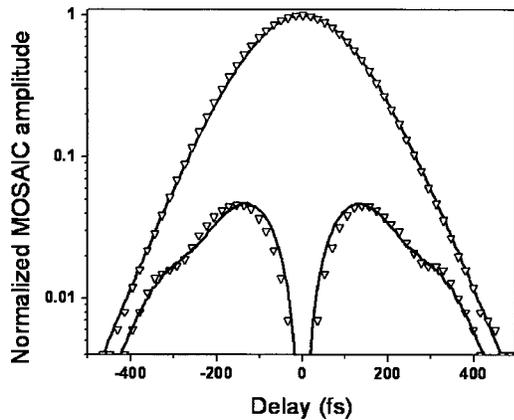
Fig. 3. Semilog plot of the experimental data (triangles) and fit (solid curves) that reveal high-order components of chirp on a 120 fs Ti:sapphire laser pulse.

[solid curves in Fig. 2, right]. This approach is very useful for characterizing ultrashort pulses deep in the ultraviolet or far infrared where the production of second-order IAC signals is often plagued by distortion and noise. Averaging also allows for efficient, *in situ* pulse monitoring, since only a relatively small amount of power needs to be diverted to the autocorrelator. It is important to emphasize that it is generally difficult to produce an averaged IAC with chirp sensitivity because of fringe jitter. Our method overcomes this obstacle.

The shoulders of the MOSAIC trace have structure and temporal separation that are sensitive measures of the order of the chirp. In Fig. 3 we fit the MOSAIC envelope in Fig. 2 (right) assuming a laser pulse having an electric field $E(t)/E_0 = \mathrm{sech}(t/t_p)\exp\{i[\omega t + \phi(t/t_p)]\}$ with chirp $\phi(t/t_p) = a(t/t_p)^2 + b(t/t_p)^3 + c(t/t_p)^4$ and pulse duration t_p. The coefficients a, b, and c are adjusted to fit to the kinks in $S_{\min}$ and the peak height. The fit shown in Fig. 3 is calculated with $a = 0.18 \pm 0.01$, $|b| = 0.2 \pm 0.02$, and $c = -0.082 \pm 0.002$. Structure in the shoulders indicates the presence of higher-order chirp (i.e., $b \neq 0$ and/or $c \neq 0$). Previous

attempts to fit a MOSAIC trace only incorporated the shoulder height.[5] The present scheme augments earlier calculated fits by the inclusion of temporal features on the MOSAIC trace. Analysis of detailed shoulder features is possible because of our newly developed averaging algorithms. The extracted information can be used to seed amplitude- and phase-retrieval algorithms such as PICASO,[7] allowing them to more rapidly converge.

In conclusion, we have shown that, by using MOSAIC, chirp extraction is possible even when IAC signals approach the noise level. The sensitivity of MOSAIC to autocorrelator misalignment, electronic bandwidth limitations, and nonquadratic detector response has been demonstrated. The ability to perform signal averaging allows us to accurately characterize the order of chirp by analyzing details of the waveform. MOSAIC continues to provide a simple approach for real-time ultrashort pulse characterization. This software is available as a free download at http://www.optics.unm.edu/sbahae/.

References

1. D. J. Kane and R. Trebino, IEEE J. Quantum Electron. **29**, 571 (1993).
2. C. Iaconis and I. A. Walmsley, IEEE J. Quantum Electron. **35**, 501 (1999).
3. A. K. Sharma, P. A. Naik, and P. D. Gupta, Opt. Express **12**, 1389 (2004).
4. J.-C. Diels and W. Rudolph, *Ultrashort Laser Pulse Phenomena: Fundamentals, Techniques and Applications on a Femtosecond Time Scale* (Academic, 1996).
5. T. Hirayama and M. Sheik-Bahae, Opt. Lett. **27**, 860 (2002).
6. M. Sheik-Bahae, Opt. Lett. **22**, 399 (1997).
7. J. W. Nicholson, M. Mero, J. Jasapara, and W. Rudolph, Opt. Lett. **25**, 1801 (2000).